Nuclear Inst, and Methods in Physics Research B 433 (2018) 69–75

Contents lists available at ScienceDirect

Nuclear Inst. and Methods in Physics Research B

journal homepage: www.elsevier.com/locate/nimb

A facility for the study of Single Event Effects in the TANDAR accelerator

M.L. Ibarra[a,*], A. Portu[b,c], G. Saint Martin[b,d], M. Barrera[a,c], A. Filevich[a,e,1], M. Alurralde[a,d]

[a] Departamento Energía Solar, Gerencia Investigación y Aplicaciones, CNEA, Argentina
[b] Departamento de Radiobiología, Gerencia de Química Nuclear y Ciencias de la Salud, CNEA, Argentina
[c] Consejo Nacional de Investigaciones Científicas y Técnicas (CONICET), Argentina
[d] Instituto Sabato, Universidad Nacional de General San Martín (UNSAM), Argentina
[e] Consultant Researcher – CNEA, Argentina

ARTICLE INFO

Keywords:
Radiation damage
Single event effects
Electrostatic accelerator
Tantalum filter
Nuclear track detector

ABSTRACT

Semiconductor devices used in space applications suffer degradation due to the space radiation environment, which affects their electric parameters, eventually reducing the in-orbit lifetime. This relatively slow behavior is due to cumulative total dose effects. On the other hand, radiation can destroy information or even damage electronic parts of the device in a sudden way. These processes are known as Single Event Effects (SEE). Heavy ion beams from electrostatic tandem or other accelerators can be used to test and characterize the response of the electronics to SEE. Two conditions are necessary for this purpose: to use very low fluxes of only a few hundred to hundreds of thousand particles/(cm^2·s), and to browse over a wide Linear Energy Transfer (LET) interval by changing the energy and/or the type of the impinging particles. In this work we describe the facility developed at the Argentine tandem accelerator (Tandar) to study SEE, and especially the fabrication and use of a perforated Ta foil to reduce the beam current to the required values. The determination of the resulting beam uniformity over the area of irradiation is also reported. The system has been tested by a SEE experiment on a webcam sensor.

1. Introduction

Space is a hostile environment for satellite components. Vacuum restricts the choice of materials that can be used and causes temperature control and charging problems. Also, wide spectrum electromagnetic radiation fields are present in space, together with energetic particles (mainly electrons, protons and cosmic rays) [1].

Electronic devices can be affected in two ways. First, a degradation of their performance is produced because of accumulation of damage in the oxide-silicon interface and in silicon due mainly to protons and electrons, the so called Total Ionizing Dose (TID) and Total Non-Ionizing Dose (TNID) [2]. A second mechanism is the occurrence of Single Event Effects (SEE), produced typically by highly ionizing particles that can deposit, directly or indirectly, huge amounts of energy in the electronic system, especially nearby sensitive zones of semiconductor devices. For example, high energy protons can produce spallation reactions with a semiconductor atom located nearby depletion layers.

The trend of the fabrication technologies towards a continuous reduction in size of the electronic devices is of particular interest for space missions, where weight, size and power consumption are the main restrictions. But the presence of ionizing radiation in space originates effects on these devices becoming more important due to the sensitive volume shrinkage and the corresponding reduction in critical charge necessary to induce effects in the device [3].

If an event produces at least a critical charge in a device, then it can generate a range of software and hardware errors. These events can be studied in the laboratory, under controlled conditions and at relatively high repetition rates to obtain adequate statistical accuracy in a reasonable amount of time. Such studies are important for the characterization and selection of existing device types, and to gain a better understanding of the phenomena involved in order to arrive at improved designs for new devices and systems.

In space the particle spectrum could reach many hundreds of MeV per nucleon. However, the relevant values of Linear Energy Transfer (LET) are limited, because the LET distribution in space reach its maximum at relatively low heavy-ion energy [1]. These energies are in the available range of the Argentine heavy ion electrostatic tandem accelerator (Tandar) [4].

Among other activities the Argentine space program, managed by

* Corresponding author.
E-mail address: ibarra@tandar.cnea.gov.ar (M.L. Ibarra).
[1] In memoriam of Alberto Filevich (1938–2018).

https://doi.org/10.1016/j.nimb.2018.07.021
Received 28 February 2018; Received in revised form 18 July 2018; Accepted 19 July 2018

the CONAE (Comisión Nacional de Actividades Espaciales/Argentine Space Agency), is devoted to the construction of satellites to study the Earth, with a special focus on the extended Argentine geography. As a part of this effort, CONAE asked the CNEA (Comisión Nacional de Energía Atómica/Argentine Atomic Energy Commission) to establish a program to qualify the radiation damage in satellite systems. CNEA's response was the creation of a group devoted to this subject, which has built a facility for the study and characterization of radiation effects.

In a previous paper, the TNID/TID facility was described [5]. The study of SEE requires special modifications of the beam line and acquisition system. This paper refers to these modifications, performed in one of the beam lines of the CNEA's Tandem Accelerator, from which a wide choice of beam species and energies are available.

A SEE experiment at a tandem accelerator requires beam intensity as low as a few hundreds of particles/(cm^2·s). This condition could lead to the so called "ghost currents", so weak, that focusing and changing energies or beam species becomes a very difficult task. The handling of this condition is not easy if a stable, controlled beam is desired. Many laboratories have implemented different solutions to this problem, such as: the use of a dispersing foil just before the analyzing magnet or an Au foil for scattering in the measurement chamber and the sample set at an adequate angular position [6–9].

The solution we have implemented at the E.D.R.A.(Ensayos de Daño por Radiación y Ambiente/Tests of Radiation and Environmental Damage) facility was to thread a normal beam current through the accelerator and then to produce a strong reduction in its intensity by installing a perforated Ta foil about 6-m before the target position. The Ta foil is thick enough to stop completely the beam particles, which can pass only through the holes. A one μm-thick Cu foil was deposited on the downstream face on the Ta foil in order to scatter the particles passing through the holes, smearing out the images of the holes and producing, after the 6-m drift space, a highly uniform particle distribution over the target area. Using this procedure, the intensity of the beam can be kept high enough in the accelerator to be easily handled and stabilized. The reduction in current is produced only downstream after the Ta foil.

2. Methodology

A SEE experiment aims at evaluating the device's response in real-time, under heavy ion or proton exposure. There are two main standards that provide a method and a test procedure for designing and performing these experiments [10,11]. Some of the principal requirements are: flux, particle type and energy, LET, beam uniformity at the sample position, beam control, and a dosimetry system [12,13]. Many particle accelerators are used with this purpose, as they provide well-characterized and almost mono-energetic beams.

Using the filters described in this work it is possible to achieve a variable flux (depending on the primary beam current and focusing condition) between a few hundred to 10^5 particles/(cm^2·s).

A beam monitoring system consisting of open BP104 PIN silicon photodiodes used as particle counters around the Device Under Test (DUT) was set to monitor the beam intensity [14].

The irradiations were performed under high vacuum condition, 10^{-5} mbar or better.

2.1. The Ta-Cu filter

To design and optimize the Ta filter, a series of Monte Carlo simulations using the TRIM code were performed [15]. TRIM produces an output file with a description of (TRANSMIT.DAT) containing atomic number, energy, position and output angle of every ion. The input data is entered in TRIM.IN that contains, among other information, the thickness of the copper foil and the irradiation conditions. The result of the simulation is obtained in the TRANSMIT.TXT output file. A code was written to process this file, to select randomly the holes and to transport the particles along the 6-m long, 20 cm diameter beam tube, up to the target position.

Prototypes were constructed using chemical etching, to evaluate the fabrication methods of this filter. From these tests we determined the etching velocity and the required size of the circles in the photolithography mask to obtain the desired final size of holes on the Ta foil. We started from a 70 μm Ta foil, which was cleaned and dried. A mask was set on one side of the sheet to obtain, inside a 25.4 mm circle, a pattern of small circles with diameters between 40 and 100 μm. The other side of the foil was then masked and the foil was etched in several steps with a 1:1 mixture of HF and HNO_3 at room temperature for 45–60 s until the desired holes were produced.

Following this procedure, we designed and produced three masks and three different tantalum filters.

1-μm thick copper foils were deposited by vacuum evaporation over glass slides. The thickness of the copper foils was measured in situ during evaporation. The foils were floated in water and then applied onto the Ta filters (downstream side) and set at their edge.

2.2. The set-up

A simplified diagram of the experimental set up is shown in Fig. 1. The Ta filters were mounted on a revolver system allowing their change without breaking the vacuum. In the irradiation chamber a target area larger than 50 × 50 mm^2 is available for SEE testing. Ions spread by the copper foil outside the central target area were used for beam monitoring and dosimetry. A mobile ring inside the chamber holds a beam shutter. When the shutter is closed, only beam measurement is allowed,

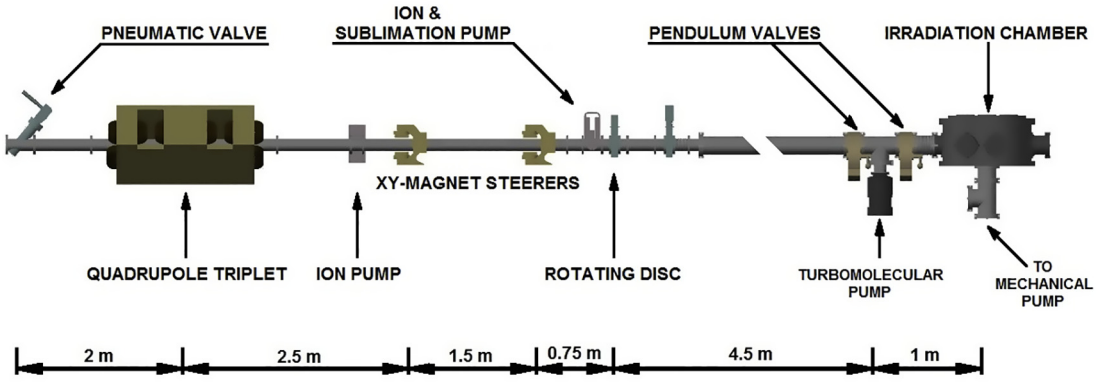

Fig. 1. A simplified E.D.R.A. beam line description showing rotating disc that hold the Ta filters and the irradiation chamber.

and when the shutter is open, beam dosimetry is still performed off center, and at the same time the beam hits the DUT.

As the flux in a SEE experiment is below the sensitivity of the Faraday Cups (FC), two silicon photodiode PIN detectors were used with pulse counting electronics. The diodes have a sensitive area of 5 mm^2, and their signals were preamplified, shaped/amplified, discriminated, and counted, using conventional NIM electronic modules. One diode is fixed nearby the DUT and the second is mobile and is installed in the front of the mobile shutter, in a position corresponding to the center of the DUT. This arrangement allows calibration and further continuous monitoring of the flux at the DUT during irradiation. For future experiments, an array of five diodes, four fixed around the DUT, and one mobile, will be set for improved beam dosimetry.

The irradiation chamber, located at the end of the beam line, was designed to perform *in-situ* experiments under high vacuum conditions and also to keep the sample at controlled temperature between −150 °C and +150 °C during irradiation.

2.3. Beam characterization

In order to characterize the beam in the irradiation chamber, after passing through the system of tantalum filters plus the copper foil, we used 250 μm thick polycarbonate foils (Lexan™) as Nuclear Track Detector (NTD) in the irradiation chamber. Each incident ion produces localized structure modifications in the polymer (nuclear tracks) due to the high energy density deposited through interaction with electrons and nuclei [16,17].

Pieces of polymer foil were irradiated with different ions and energies using the three Ta filters, with and without the dispersing copper foil. To reveal the tracks, a PEW (30 g KOH + 80 g CH_3CH_2OH + 90 g H_2O) solution at 70 °C was used for 2-min chemical etching. The foils were observed in an optical microscope with a motorized stage (Lanais MEF, CNEA-CONICET, Carl Zeiss MPM 800, 40x) [18]. For each polymer foil, 72 micrographs of 200 μm × 160 μm were taken in an (9x8) matrix with 5 mm spacing.

The tracks in each micrograph were counted and their (x, y) coordinates were recorded.

The distribution of tracks on the micrograph was studied by application of spatial statistics. The spatial data analysis were performed with R, a free software environment for statistical computing and graphics [19]. The *spatstat* package, which contains functions for manipulating and representing data, as well as statistical functions for analyzing point data, was also used [20].

3. Results and discussion

3.1. Filter prototype

Filter prototypes were fabricated and characterized using an optical profilometer and a scanning electron microscope (Fig. 2) [21]. The etching velocity was 4 μm/min, and the final shape of the hole's walls was conical. This shape helps avoiding scattering problems with the ion beam that could appear in the case of holes with straight walls.

Three filters were built, each one with different number and diameter of holes (see Table 1). In all cases the hole diameters were determined using an optical microscope. The transmission factor was calculated as the ratio of the total open area to the total area of the filter. The filters were installed in the E.D.R.A. beam line at about 6 m before the target position, providing enough drift space for the beam to be dispersed, producing a nearly uniform irradiation over a large target area. However, to achieve this purpose, copper foils of 1 μm thickness had to be attached on the downstream faces of the Ta foils.

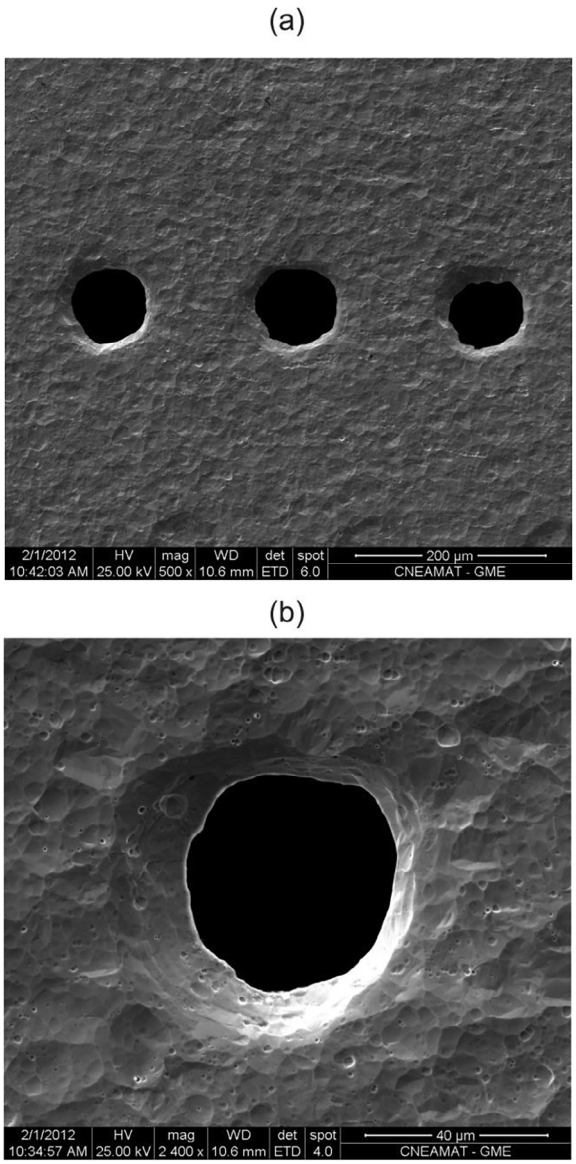

Fig. 2. Scanning electron micrograph of (a) downstream face and (b) upstream face of the prototype tantalum etched foil.

Table 1
Characteristics of the tantalum filters.

Filter	Ta thickness (μm)	Perforation number	Perforation average diameter (μm)	Perforation number/cm^2	Transmission factor
Ta1	70	31	100	6.1	$4.81\ 10^{-4}$
Ta2	50	73	130	14.4	$1.91\ 10^{-3}$
Ta3	50	31	70	6.1	$2.35\ 10^{-4}$

3.2. Characterization of the beam profile by using a nuclear track-sensitive polymer

Several experiments were performed in order to study the ion beam uniformity after passing through the Ta filter and Ta-Cu filters. Polymer foils of 50 mm × 50 mm were irradiated with 50 MeV ^{16}O and 83 MeV ^{127}I ions. These beam species were selected as representative of SEE experiments, their respective LET values being 4.6 to 41.8 MeV/(mg·cm^2).

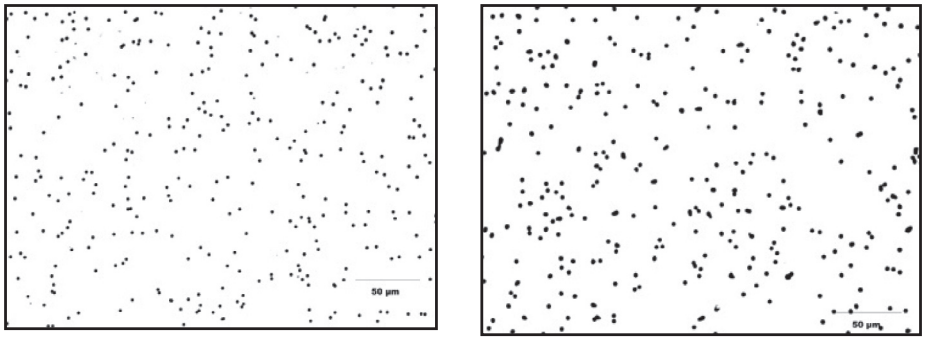

Fig. 3. Examples of optical micrographs of polymer irradiated with Ta1-Cu filter and (a) 50 MeV ^{16}O (b) 83 MeV ^{127}I.

A simple procedure is used for adjusting the beam optics elements to guide the beam and to hit the center of the irradiation chamber. This is firstly done using an empty foil holder in the rotating disc and observing the beam spot produced on a phosphor paint screen applied on the surface of the FC's front plate. A quadrupole triplet and a pair of magnetic steerers allow focusing and directing the beam along the tube and center it at the target position. Once the beam is collected by the FC, the rotating disc is adjusted to set the tantalum filter selected for the experiment in front of the beam.

In order to assess the behavior of the dispersing filter a beam intensity was chosen and set using the PIN diodes, to produce, in average, a track density of about 10^6 particles/cm^2 over the polymer foil area. This value of track density was selected in order to avoid overlapping of tracks on the polymer surface, allowing observation and counting under microscope.

The effects of the Ta filter followed by the Cu foil have been tested in several runs performed using Ta3 filter with and without the Cu foils. It can be observed that, without the dispersing Cu foil, the distance of almost 6-m between the filter and the irradiation chamber is not enough to obtain a uniform ion beam on the target.

Several runs were performed using 50 MeV ^{16}O, and 83 MeV ^{127}I beams and the three Ta-Cu filters, which were characterized and monitored using the described PIN detectors. The accelerator current was adjusted between 0.2 and 6.0 nA, and the obtained density of tracks on the polymer foil varied between 170 and 3800 tracks/cm^2.

In order to evaluate the degree of dispersion of the beam particles and the beam uniformity, micrographs of all irradiated polymer foils were taken. The experiment results with the three filters and different ion beams were similar (examples are shown in Fig. 3). 72 images were obtained and the number of tracks in each micrograph was counted. The number of tracks measured at each position of the whole detector surface was plotted versus their (x,y) coordinates on the polymer foil (Fig. 4).

To explore an eventual dependence between events, we used the estimates of the Ripley's reduced second moment function K(r), the empty space function F(r) and the pair correlation function g(r) [22,23]. The Ripley's K(r) function measures the number of events found up to a given distance r of any other particular event. The K function is defined so that λK(r) equals the expected number of random points within a radius r of a typical random point. For a Complete Spatial Randomness (CSR) process:

$$K_{CSR}(r) = \pi r^2$$

The experimental K function deviates from the theoretical expected value (K_{CSR}) assuming the points are completely random. While $K > K_{CSR}$ suggests clustering, $K < K_{CSR}$ suggests pattering (Fig. 5).

The empty space function F, is the cumulative distribution of the distance from a fixed point in space to the nearest point. For a CSR process with intensity λ:

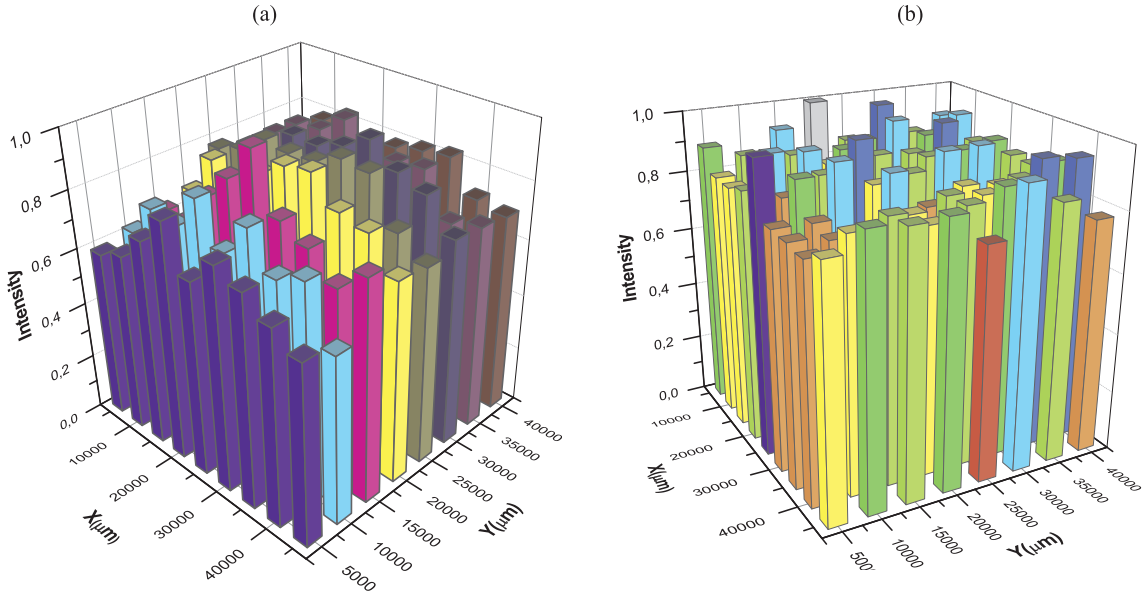

Fig. 4. Uniformity measurement: tracks intensity (count number divided by the maximum count number observed) in a 50 × 50 mm^2 polymer foil irradiated with (a) 50 MeV ^{16}O (with Ta1 filter), and (b) 83 MeV ^{127}I (with Ta2 filter) respectively.

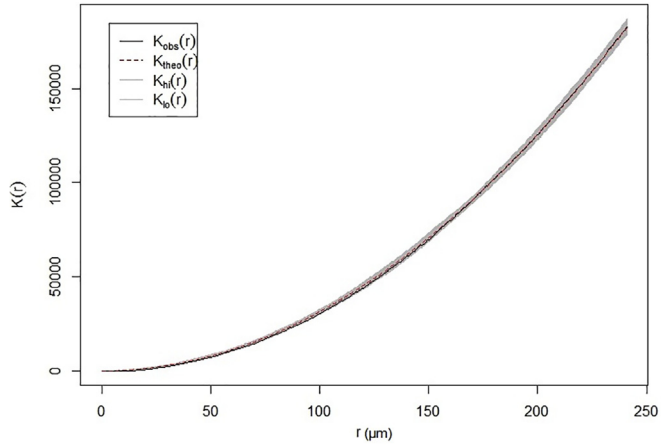

Fig. 5. K(r) function. "Obs" corresponds to the experimental and "Theo" to the theoretical curve for a complete spatially random process. "hi" and "lo" are the limits obtained from Monte Carlo simulation.

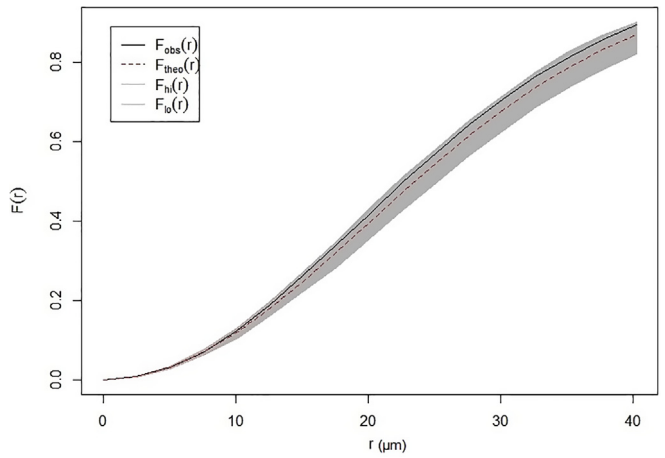

Fig. 6. F(r) functions. "Obs" correspond to the experimental and "Theo" to the theoretical curve for a complete spatial randomness process. "hi" and "lo" are the limits obtained from Monte Carlo simulation.

$$F_{CSR}(r) = 1 - \exp(-\lambda \pi r^2)$$

While $F > F_{CSR}$ suggests that empty space distances are shorter than for a CSR process (regularly space pattern), $F < F_{CSR}$ suggests a clustered pattern. The theoretical curve is computed using F_{CSR} and the experimental curve is found using the point locations (Fig. 6).

To test whether this deviation is statistically significant, the standard approach is to use a Monte Carlo test based on envelopes of the K and F function obtained from simulated point patterns (Figs. 5 and 6).

The pair correlation function g(r) is the derivate of Ripley's function, K(r), and is equal to one for CSR (Fig. 7). This function expresses the probability of observing a pair of points separated by a distance r divided by the corresponding probability for CSR process. Values of $g(r) < 1$ suggest inhibition or regularity between tracks and values greater than 1 suggest clustering or attraction at distance r. The exploratory analysis concluded that the there is no regularity or clustering in the observed area of the polymer foil.

To verify that the tracks are distributed independently at random and uniformly over the study area, we performed several tests, such as the Quadrat Counting (QC) and the Kolmogorov-Smirnov (K-S) [22,23]. QC is a χ^2 test where CSR is the null hypotheses (Ho) and the alternative is aggregation or regularity. In this test the window A is divided into sub regions (*quadrats*) of equal areas, and the number of data points in each tile is counted (Fig. 8). The expected number of points in each quadrat is also calculated, as determined by CSR. Then we perform a two tails χ^2 test of goodness-of-fit to the quadrat counts.

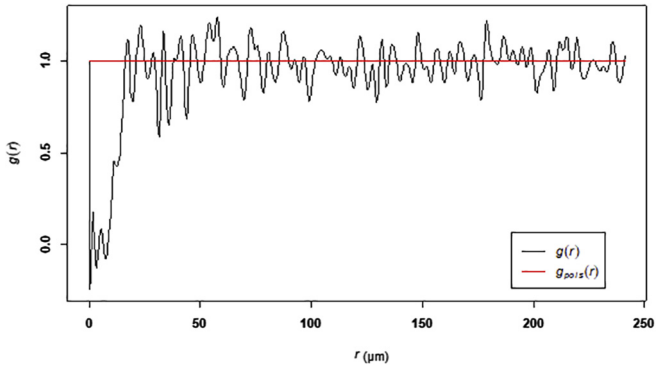

Fig. 7. Pair function correlation g(r). "g(r)" correspond to the experimental and "$g_{pois}(r)$" to the theoretical curve for a complete spatial randomness process.

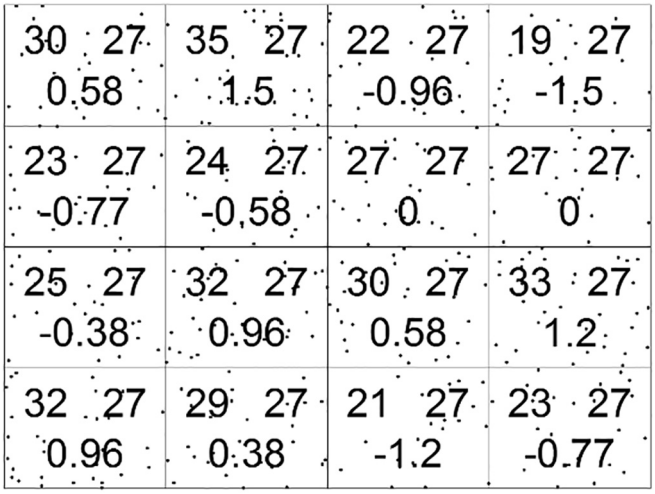

Fig. 8. QC test distributions where the observed counts n_j are at top left; expected count are at top right and Pearson residuals at bottom.

For all the samples, the Ho was accepted with 99.95% [22].

The K-S test compares the observed and predicted distributions of the values of some function T. A real-valued function T(x, y) is defined at all locations (x, y) in the window. Then, the function is evaluated at each one of the data points. Finally, the experimental value of T is compared with the predicted distribution of values of T under CSR. The null hypothesis is simply H_0: "the model fits the data". The p-value in the two tests accepts the null hypothesis (Figs. 9 and 10).

The exploratory analysis and hypothesis test were performed in

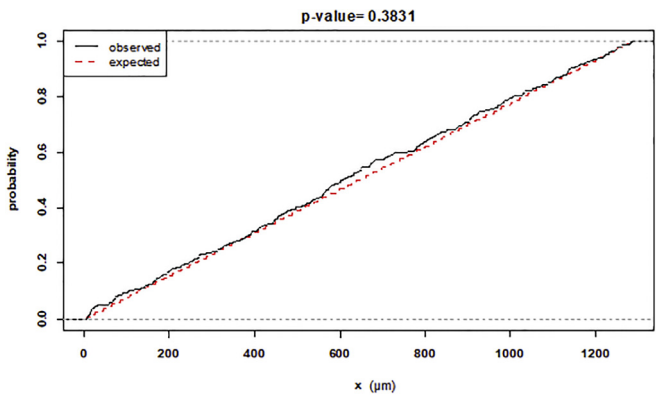

Fig. 9. K-S test distributions for x coordinates.

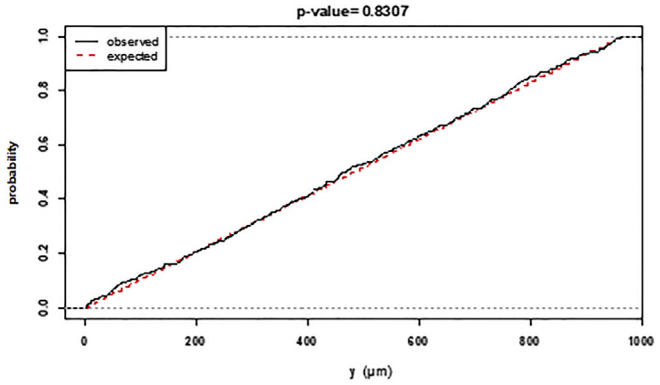

Fig. 10. K-S test distributions for *y* coordinates.

each of the 72 micrographs for every irradiated polymer foil. The results in all cases agree with CSR.

Finally, we used the Kruskal-Wallis rank sum test where the null hypothesis is that "the distributions are the same in each group, while the alternative is that they differ in at least one". As well as the other tests, Ho was accepted.

The same statistical analysis was performed on the results of the Monte Carlo simulations using the ions and energies of the experimental irradiations. The results agree with the Complete Spatial Randomness observed in the experimental data.

The ESA norm for SEE testing requires a beam uniformity of 10% [24]. As shown in Table 2, most of the target areas fulfill the condition.

4. SEE observed on a webcam sensor

In order to test the capabilities of the filter system we irradiated a webcam sensor, whose simplicity of observation is one of the main advantages of this type of devices. However, the sensor was protected by a 400 μm plastic film, which is very difficult to remove without damaging it. This fact constitutes a disadvantage, because it avoids the use of oxygen or iodine beams, which cannot reach the sensitive area. To overcome this problem, we used in this case an 8 MeV proton beam. Despite that protons cannot be stopped by the 70 μm Ta foil, neither at the plastic film, the energy loss was so important that only the protons going through the holes have enough energy to excite the sensor; the rest of them were not detected. The webcam sensor of 0.12 cm^2 was irradiated with 8 MeV protons using the three Ta filters with copper foil. A 100-s film video was recorded for each Ta-Cu filter. In order analyze the results the films were separated into frames. Statistical tools have been used to assess the randomness and uniformity of the illuminated pixel distribution (Figs. 11 and 12).

Fig. 13a shows the image sensor response to protons. Each proton was registered as a white dot whose diameter is around 49 pixels

Table 2
Beam uniformity for different filters, ions and target areas. The beam uniformity was calculated as the ratio between the standard deviation and the average track density in the selected area.

Filter	Ion	10 × 10 mm^2 Beam uniformity (%)	20 × 20 mm^2 Beam uniformity (%)	50 × 50 mm^2 Beam uniformity (%)
Ta1	^{16}O	3	6	11
	^{127}I	7	6	6
Ta2	^{16}O	9	8	11
	^{127}I	5	5	5
Ta3	$^{16}O^{*}$	–	–	–
	^{127}I	5	4	4

* This experiment was performed using Ta3 without the copper foil.

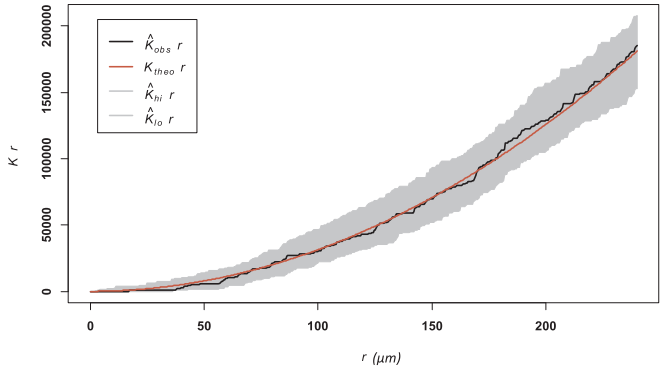

Fig. 11. K(r) function. "Obs" correspond to the experimental and "Theo" to the theoretical curve for a complete spatial randomness process. "hi" and "lo" are the limits obtained from Monte Carlo simulation.

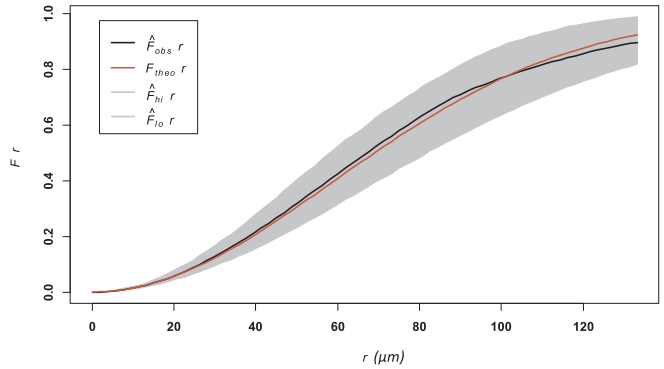

Fig. 12. F(r) function. "Obs" correspond to the experimental and "Theo" to the theoretical curve for a complete spatial randomness process. "hi" and "lo" are the limits obtained from Monte Carlo simulation.

square. Magnification of one trace is shown in Fig. 13b. Due to deposition of a high amount of energy in the image sensor, the phenomenon of blooming occurred. The charge generated by a single proton diffuses to potential wells involving about 50 surrounding pixels.

5. Conclusions

In this work we describe a facility designed to evaluate in real-time the sensitivity to SEE of electronic devices for space environment. In order to achieve the experimental conditions to perform a SEE experiments, a set of Ta-Cu filters were designed, constructed and installed in the beam line.

Monte Carlo simulations were made to design and optimize the Ta-Cu filter. Micro and nanofabrication techniques were used to achieve a geometric array of perforations on a tantalum foil. A copper foil is used as a dispersive tool to spread the beam uniformly over the sample area.

To test the filter attenuation factors and the uniformity of the ion beam at the target, nuclear track detectors were irradiated. Spatial statistics analyses were applied to the data obtained from NTD. Several tests concluded that no regularity or clustering was present on the 50 × 50 mm^2 area of study. The beam uniformity was verified and the complete spatial randomness of the tracks was accepted with 99.95% of confidence. The Ta-Cu system satisfies the beam uniformity required for SEE experiments.

Finally, in order to test the system, we performed SEE experiments on a webcam using 8 MeV protons. A 100-s film was recorded with each Ta-Cu filter. The films were separated into frames and a spatial statistical analysis concluded that illuminated pixels were uniformly and randomly distributed.

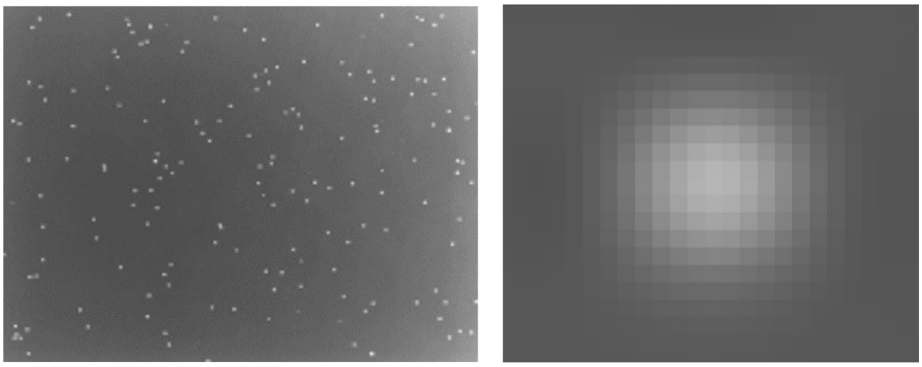

(a) (b)

Fig. 13. (a) Webcam sensor response for protons, (b) Trace left by one proton.

References

[1] A. Holmes-Siedle, L. Adams, Handbook of Radiation Effects, second ed., Oxford University Press, New York, 2002.

[2] R. Velazco, P. Fouillat, R. Reis (Eds.), Radiation Effects on Embedded Systems, Springer, Netherlands, 2007.

[3] E.A Burke, The Impact of Component Technology Trends on the Performance and Radiation Vulnerability of Microelectronic Systems, IEEE NSRE Conf. Short Course, (1985).

[4] E. Perez Ferreira, M.A.J. Marisctoyi, E. Ventura, A. Ceballos, N. Fazzini, A. Filevich, H. Gonzalez, R. Requejo, R. Ribarich, J.J. Rossi, E. Achterberg, D. Camin, J. Nicolai, S. Tau, The argentine 20 MV Tandem Accelerator Project, Nucl. Instrum. Methods 184 (1981) 161–172, https://doi.org/10.1016/0029-554X(81)90863-6.

[5] A. Filevich, C.J. Bruno, J.F. Vázquez, M. Alurralde, I. Prario, M.J.L. Tamasi, et al., A compact portable setup for in situ solar cells degradation, IEEE Trans. Nucl. Sci. 50 (2003) 2380–2384, https://doi.org/10.1109/TNS.2003.821580.

[6] P. Thieberger, E.G. Stassinopoulos, V. Gunten, V. Zajic, Heavy-ion Beams for Single-Event Research at Brookhaven – Present and Future, 56-57 (1991) 1251–1255. https://doi.org/10.1016/0168-583X(91)95144-3.

[7] V. Zajic, P. Thieberger, Heavy ion linear energy transfer measurements during single event upset testing of electronic devices, IEEE Trans. Nucl. Sci. 46 (1999) 59–69, https://doi.org/10.1109/23.747768.

[8] V.A.P. Aguiar, N. Added, N.H. Medina, E.L.A. Macchione, M.H. Tabacniks, F.R. Aguirre, M.A.G. Silveira, R.B.B. Santos, L.E. Seixas Jr., Experimental setup for single event effects at the São Paulo 8UD pelletron accelerator, Nucl. Instrum. Methods Phys. Res. Sect. B Beam Interact. Mater. Atoms. 332 (2014) 397–400, https://doi.org/10.1016/j.nimb.2014.02.105.

[9] H.E. Chao-hui, Y. Hai-liang, G. Bin, C. Xiao-hua, Z. Zheng-xuan, L.I. Guo-zheng, L. Guo-zheng, Experimental study on Single Event Effects in Semiconductors Devices Using Accelerators, Proceedings, 2nd Asian Conference, APAC'01, Beijing, P.R. China, (2001) 923–925.

[10] J.R. Schwank, M.R. Shaneyfelt, P.E. Dodd, Radiation hardness assurance testing of microelectronic devices and integrated circuits: test guideline for proton and heavy ion single-event effects, IEEE Trans. Nucl. Sci. 60 (2013) 2101–2118, https://doi.org/10.1109/TNS.2013.2261317.

[11] R.A. Reed, J. Kinnison, J.C. Pickel, S. Buchner, P.W. Marshall, S. Kniffin, K.A. LaBel, Single-event effects ground testing and on-orbit rate prediction methods: the past, present, and future, IEEE Trans. Nucl. Sci. 50 (2003) 622–634, https://doi.org/10.1109/TNS.2003.813331.

[12] DOD, MIL-STD-883E Test Method Standard – Microcicrcuits, Mil-Std. 570 (1996).

[13] V. Ferlet-Cavrois, J.R. Schwank, S. Liu, M. Muschitiello, T. Beutier, A. Javanainen, et al., Influence of beam conditions and energy for SEE testing, IEEE Trans. Nucl. Sci. 59 (2012) 1149–1160, https://doi.org/10.1109/TNS.2012.2187681.

[14] V. Semiconductors, Vishay Semiconductors Silicon PIN Photodiode, RoHS Compliant Test Condition Symbol Silicon PIN Photodiode, RoHS Compliant SYMBOL, (2002) 386–390.

[15] J.F. Ziegler, J.P. Biersack, SRIM: The Stopping and Range of Ions in Matter. http://www.srim.org/.

[16] S.A. Durrani and R.K. Bull. Solid State Nuclear Track Detection. Principles, methods and applications. (1987) International Series in Natural Philosophy. Ed. D. ter Haar, Pergamon Press, Oxford.

[17] G. Saint Martin, A. Portu, G.A. Santa Cruz, O.A. Bernaola, Stochastic simulation of track density in nuclear track detectors for 10B measurements in autoradiography, Nucl. Instrum. Methods Phys. Res. Sect. B Beam Interact. Mater. Atoms. 269 (2011) 2781–2785, https://doi.org/10.1016/j.nimb.2011.08.031.

[18] A. Portu, M. Carpano, A. Dagrosa, R.L. Cabrini, G. Saint Martin, Qualitative auto-radiography with polycarbonate foils enables histological and track analyses on the same section, Biotechnic Histochem.y 88 (5) (2013) 217–221, https://doi.org/10.3109/10520295.2012.759624.

[19] R Development Core Team, R: A Language and Environment for Statistical Computing, (2011). http://www.R-project.org/.

[20] A. Baddeley, Analysing spatial point patterns in R, Work. Notes. 12 (2008) 1–199. doi: 10.1007/s00415-011-6369-2.

[21] M.L. Ibarra, B. Cetrángolo, M. Barrera, Elaboración y Caracterización de un Atenuador de Corriente para la Línea E.D.R.A. del Acelerador TANDAR, Acta Microsc 21 (2012) 125–126.

[22] J. Illian, A. Penttinen, H. Stoyan, D. Stoyan, Statistical analysis and modelling of spatial point patterns, Wiley (2008), https://doi.org/10.1002/9780470725160.

[23] A. Baddeley, R. Turner, spatstat: an R package for analyzing spatial point patterns, J. Stat. Softw. 12 (2005) 1–42 10.1.1.126.8464.

[24] Single Event Effects Test Method and Guidelines, Document Custodian: European Space Agency, ESCC Basic Specification No. 25100, (2014). https://escies.org.